THE JOURNAL OF PHYSICAL CHEMISTRY B
A JOURNAL OF THE AMERICAN CHEMICAL SOCIETY

pubs.acs.org/JPCB

Article

Molecular Structure of the Surface-Immobilized Super Uranyl Binding Protein

Wen Guo, Xingquan Zou, Hanjie Jiang, Karl J. Koebke, Marie Hoarau, Ralph Crisci, Tieyi Lu, Tao Wei,* E. Neil G. Marsh,* and Zhan Chen*

Cite This: *J. Phys. Chem. B* 2021, 125, 7706–7716

Read Online

ACCESS | Metrics & More | Article Recommendations | Supporting Information

ABSTRACT: Recently, a super uranyl binding protein (SUP) was developed, which exhibits excellent sensitivity/selectivity to bind uranyl ions. It can be immobilized onto a surface in sensing devices to detect uranyl ions. Here, sum frequency generation (SFG) vibrational spectroscopy was applied to probe the interfacial structures of surface-immobilized SUP. The collected SFG spectra were compared to the calculated orientation-dependent SUP SFG spectra using a one-excitonic Hamiltonian approach based on the SUP crystal structures to deduce the most likely surface-immobilized SUP orientation(s). Furthermore, discrete molecular dynamics (DMD) simulation was applied to refine the surface-immobilized SUP conformations and orientations. The immobilized SUP structures calculated from DMD simulations confirmed the SUP orientations obtained from SFG data analyzed based on the crystal structures and were then used for a new round of SFG orientation analysis to more accurately determine the interfacial orientations and conformations of immobilized SUP before and after uranyl ion binding, providing an in-depth understanding of molecular interactions between SUP and the surface and the effect of uranyl ion binding on the SUP interfacial structures. We believe that the developed method of combining SFG measurements, DMD simulation, and Hamiltonian data analysis approach is widely applicable to study biomolecules at solid/liquid interfaces.

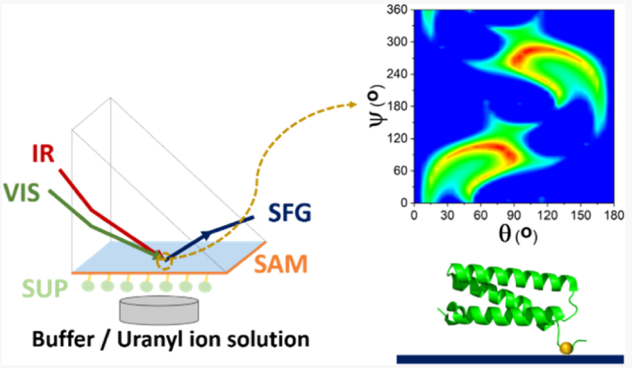

INTRODUCTION

Proteins and peptides play important roles in a broad range of applications, ranging from biosensing,[1−3] tissue engineering,[4] drug development,[5,6] and so forth. They can effectively bind metal ions, interact with different molecules and genes,[2,7,8] and catalyze biochemical reactions.[9,10] The functions of proteins and peptides are mediated by their structures. This research is aimed at developing a combined experimental, computation simulation, and spectral calculation method to deduce a surface-immobilized protein structure using a recently designed protein for uranyl ion detection as an example. Uranium is one of the main sources in nuclear energy generation and is also known to cause acute toxicological effects in mammals as a carcinogenic agent. Therefore, it is necessary to develop simple methods with excellent sensitivity and specificity to detect and harvest uranyl ions. Various analytical methods have been used to detect uranyl ions, including optical spectroscopy (e.g., fluorescence spectroscopy,[11] spectrophotometry,[12] optode,[13] and Raman spectroscopy[14,15]), mass spectrometry,[16] separation methods,[17] and electrochemical analysis.[18−20] Recently, various methods using biological molecules to detect uranyl ions have also been developed.[21,22] Zhou et al.[23] previously reported an α-helical peptide, called super uranyl binding protein or SUP, that binds UO_2^{2+} with femtomolar affinity and remarkable selectivity, better than 10,000-fold affinity over other common metal ions. The X-ray structure of this peptide was determined with both UO_2^{2+} absent (PDB ID: 4FZO) and bound (PDB ID: 4FZP) and revealed that the SUP conformation changes only slightly in response to UO_2^{2+}-binding. The design and test of SUP for uranyl ion binding shed light on effective uranyl ion detection and harvesting. To facilitate the incorporation of SUP into a device to detect or bind uranyl ions, it is necessary to immobilize SUP on a solid surface with desired orientation for better sensitivity, stability, reusability, and localization.[24,25] The immobilization strategies of proteins and peptides (e.g., enzymes and antimicrobial peptides) have been well developed over the last decades,[26−31] including noncovalent interactions (such as physical adsorption and ionic attraction) and covalent

Received: April 29, 2021
Revised: June 29, 2021
Published: July 13, 2021

https://doi.org/10.1021/acs.jpcb.1c03849
J. Phys. Chem. B 2021, 125, 7706–7716

attachment. The noncovalent methods, while simple, have leaching problems and often decrease the activity of the immobilized proteins and peptides due to the lack of orientation control for proteins and peptides to adopt favorable orientations on the surface. One of the covalent attachment methods is to connect a unique cysteine residue on the surface of a protein or peptide to the substrate surface through the thiol−maleimide interaction,[25,32−34] which can tune and balance the flexibility and rigidity of the immobilized protein or peptide to adopt a proper conformation and orientation on the surface. We have extensively investigated proteins and peptides immobilized using this method.[25,32−34] It has been demonstrated that self-assembled monolayers (SAMs) and functionalized polymers can be used as solid substrates to immobilize proteins and peptides to adopt a desired conformation and/or orientation.[24,25,34−45]

Protein structures in the bulk environments such as those in solutions or crystal form have been extensively studied using X-ray and NMR methods. However, it is challenging to investigate protein structures at solid/liquid interfaces in situ due to the lack of appropriate analytical techniques. Recently, a surface-sensitive technique, sum frequency generation (SFG) vibrational spectroscopy, has been demonstrated to be a powerful method to elucidate protein structures at interfaces,[43,46] but a systematic approach for data analysis and structural determination for SFG experimental results is needed.

In this research, we engineered a SUP mutant, designated SUP-C105, which contains a unique cysteine residue at the C-terminus to allow it to covalently bind to a maleimide-terminated SAM surface. To better understand interactions between the SAM substrate and the immobilized SUP protein and thereby facilitate the development of better immobilization strategies, we applied SFG to investigate the surface-immobilized SUP structure both before and after binding the uranyl ion. Previous research shows that free SUP in solution exhibits a substantial structural change after uranyl ion binding,[47] while the crystal structures of the SUP with and without uranyl ion binding are very similar.[23] The crystal environment is more constrained compared to the solution environment. The SFG results will reveal the effect of the surface immobilization (or surface−SUP interaction) on SUP structural changes before and after uranyl ion binding. In this study, two additional methods, discrete molecular dynamics (DMD) simulation and one-excitonic Hamiltonian approach (here exciton means vibrational exciton) for SFG spectral simulation, were adopted to correlate with the SFG results to determine the molecular structure of SUP-C105 immobilized on the SAM surface. Here, the molecular structure refers to the conformation and orientation of the interfacial protein.

EXPERIMENTAL SECTION

SUP Expression and Purification. *Escherichia coli* codon-optimized gene encoding SUP with a 6-His tag within pET28a was mutated to SUP C31S C87S I105C (SUP-C105) using the same cell transformation, culture and harvest, and SUP purification methods as those reported in the published protocol.[47] The SUP-C105 sequence is as follows: SLDSRER-IEKDLEDLEKELMEMSIKLSDDEEAVVERALNYRDDS-VYYLEKGDHITSFGSITYAEGLTDSLRMLHRICEG. Samples were stored at −80 °C until use.

SAM Preparation. The SiO_2-coated CaF_2 prisms were obtained by previously published methods.[25,32−34] These prisms were oxygen plasma treated for 30 s to functionalize the SiO_2 surface with hydroxyl groups to react with *O*-(propargyl)-*N*-(triethoxysilylpropyl)carbamate in anhydrous toluene solution in the dark for 24 h. After rinsing the prisms with toluene, ethanol, and Millipore water twice, the prisms were placed into a 1 mM azido-PEG3-maleimide linker (Click Chemistry Tools, AZ107-10) solution containing copper ions for 24 h at room temperature to grow a maleimide-terminated monolayer. Excess copper ions were removed by 200 mM ethylenediaminetetraacetic acid solution, and then, the prisms were rinsed with Millipore water twice. The maleimide-terminated SAMs on the prisms were immersed in 2.5 μM SUP solutions (5 mM potassium phosphate buffer with pH = 7.4) overnight for SUP immobilization.

SFG Spectroscopy. SFG is a second-order nonlinear optical process characterized by second-order nonlinear optical susceptibility $\chi^{(2)}$.[40,41,43,44,48−78] SFG theories, experimental setups, and data analyses have been extensively reported[40,41,43,44,48−78] and will not be repeated here. Under the electric dipole approximation, the SFG signal cannot be generated from most bulk materials which have inversion symmetry but can be produced from surfaces/interfaces where inversion symmetry is broken.[40,41,43,44,48−78] For the SFG near-total-reflection setup (Supporting Information, Figure S1) used in this study, two input laser beams, a fixed 532 nm visible beam and a tunable mid-infrared beam (1100 to 4300 cm^{-1}), temporally and spatially overlapped at the sample interface to generate a sum frequency ($\omega_{sum} = \omega_{vis} + \omega_{IR}$) signal beam.[40,41,43,44,48−78] In this research, SFG amide I signals can only be generated from the immobilized SUP protein molecules at the solid/liquid interface, even though the penetration depths of the input beams are much larger. The overlap area of the input beams is a round spot with 500 μm in diameter. Therefore each SFG amide I spectrum was collected from the immobilized protein molecules at the solid/liquid interface within a round area of 500 μm. The resolution of the SFG spectrometer used is 5 cm^{-1}. In the collected SFG spectra, the peak centered at ∼1650 cm^{-1} indicates the presence of an α helical structure in a protein/peptide.[79] The orientation of the detected protein/peptide at the interface can be deduced from the ratio of $\chi^{(2)}$ values obtained from ssp- (s-polarized SFG signal, s-polarized input visible beam, and p-polarized input IR beam) and ppp-polarized spectra ($\chi^{(2)}_{ppp}/\chi^{(2)}_{ssp}$).[80−82]

The SFG spectra can be fitted using the standard method with the following equations[63,66]

$$I(\omega) \propto |\chi^{(2)}_{eff}|^2 = \left|\chi_{NR} + \sum_q \frac{A_q}{\omega_2 - \omega_q + i\Gamma_q}\right|^2 \quad (1)$$

Here, $I(\omega)$ is the SFG spectral intensity. $\chi^{(2)}_{eff}$ is the effective second-order nonlinear susceptibility tensor at the surface or interface. χ_{NR} is the nonresonant contribution. A_q, ω_q, and Γ_q are the signal strength, the vibrational frequency, and the damping coefficient of the vibrational mode q, respectively.

The $\chi^{(2)}_{ppp}/\chi^{(2)}_{ssp}$ (measured in the experiments) can be obtained from the fitted ssp and ppp SFG spectra, from which the $\chi^{(2)}_{zzz}/\chi^{(2)}_{yyz}$ (defined in the lab-fixed coordination system) value can be deduced ($\chi^{(2)}_{ppp}/\chi^{(2)}_{ssp} = 0.9 \times \chi^{(2)}_{zzz}/\chi^{(2)}_{yyz}$).[83] The ssp and ppp SFG spectra of the immobilized SUP molecules were at first collected from the substrate (with SUP immobilized)/phosphate buffer (PB) solution (5 mM with pH

https://doi.org/10.1021/acs.jpcb.1c03849
J. Phys. Chem. B 2021, 125, 7706−7716

= 7.4) interface in the frequency region of 1500−1800 cm^{-1}. Then, the PB solution in contact with the SAM substrate (with SUP immobilized) was replaced by a uranyl ion solution (100 μM uranyl ion in PB solution), and the ssp and ppp SFG spectra were collected from the immobilized SUP molecules at the substrate (with SUP immobilized)/uranyl ion solution interface in the same frequency region after the SFG signals became stable.

Hamiltonian Approach. In the past, we used SFG signals contributed from the α-helical structure to determine the protein orientation.[25,82,84] In this research, we adopted a Hamiltonian method to determine the protein interfacial orientation (the tilt angle θ and the twist angle ψ) using SFG spectra contributed from the entire protein.[72,85] For the Hamiltonian method, we first used each amino acid in the protein as a basis to construct the Hamiltonian matrix. The diagonal terms of this matrix are the uncoupled amide I vibration mode peak center. Coupling between each pair of amino acids can be calculated according to the distance and orientation of the amino acids (with the known protein structure) and used as the off-diagonal terms. The Hamiltonian matrix can then be diagonalized, with the diagonal terms as the new peak centers and the new basis for each mode is a combination of the amino acids. The signal strength of each mode is then calculated for each peak center. Using a reasonably assumed peak width for each mode, the SFG spectrum of the protein can be constructed for a specific orientation. Then, the protein can be rotated, and the *zzz* and *yyz* SFG spectra were calculated as a function of the protein orientation (θ, ψ). The assigned local frequencies and peak widths for the spectral calculation were obtained from experimental SFG fitted results (Supporting Information, S2). In this research, we calculated the SFG spectra of the SUP proteins with θ between 0 and 180° and ψ between 0 and 360°, with a step of 5° for θ and ψ. These calculated SUP orientation-dependent SFG spectra were compared to the experimental SFG data to deduce SUP orientation. For the first time, a quantitative score system was developed in the Hamiltonian program to evaluate matching qualities of the five matching standards (for more details, see below) between calculated and experimentally collected SFG spectra.

To save computational time, we first filtered out the calculated SFG spectra (*zzz* or *yyz*) that have more than one peak and whose r^2 values of the fitting are lower than 0.8. Spectra that survived this filtering standard are possible candidates, which we match against experimental spectra (each experimentally collected ppp or ssp spectrum only contains one peak). Score 1 and score 2 evaluated the propinquity between experimentally observed peak centers in ppp and ssp spectra and calculated peak centers of *zzz* and *yyz* spectra, respectively. Good matching is defined as a difference between the calculated and observed peak center within ±5 cm^{-1} (score > 0.9). Score 3 and score 4 assessed the similarity between experimental peak widths of the ppp and ssp spectra and simulated peak widths of the *zzz* and *yyz* spectra. Only calculated spectra with a peak width within ±20% of the experimental value were scored, and a score higher than 0.9 means that the deviation is less than ∼5 cm^{-1}. Score 5 compared the $\chi^{(2)}_{zzz}/\chi^{(2)}_{yyz}$ ratios between experimentally deduced and theoretically deduced values, with a tolerance of ±20% of the experimentally deduced value. The final matching score is the product of all five scores mentioned above. A good overall matching is defined as a final matching score higher than 0.59 (if on average each score is 0.9, the final score is 0.9 × 0.9 × 0.9 × 0.9 × 0.9 = 0.59). Calculation details of Hamiltonian approach and detailed formulas of this score system can be found in the Supporting Information (S3).

DMD Simulations. DMD simulations were performed using the software package (sDMD) developed by Zheng and co-workers.[86,87] In our simulations, the intra- and intermolecular interactions of protein(s) in the aqueous environment were represented precisely in an implicit water environment using well-calibrated all-atom DMD forcefield parameters published in the literature.[88] Interactions between protein residues and the substrate surface were computed efficiently using the coarse-grained Go-like model[89−91]

$$V_{\text{surface}} = \sum_{i}^{N} \left\{ \pi\rho\sigma_i^3\epsilon_i \left[\theta_1 \left(\frac{\sigma_i}{z_{is}}\right)^9 - \theta_2 \left(\frac{\sigma_i}{z_{is}}\right)^7 + \theta_3 \left(\frac{\sigma_i}{z_{is}}\right)^3 - (\theta_s\chi_s + \theta_p\chi_{pi}) \left(\frac{\sigma_i}{z_{is}}\right)^3 \right] \right\}$$

where N stands for the residues' number in a protein, z_{is} is the distance between residue I and the surface, and σ_i and ϵ_i are the van der Waals parameters. To account for the hydrophobic effects of the SAM surface, the surface's hydrophobic index χ_s was set to 4.5[91] and the value (χ_{pi}) of the amino acid i was taken from the literature.[92] The parameters (θ_1, θ_2, θ_3, θ_s, and θ_p) were obtained from the previous study.[91] It is notable that the Go-like model has been successfully used in our previous studies[42,89,93−95] to predict protein/peptide orientation and structure on SAMs, polymers, and two-dimensional material (e.g., graphene or MoS_2) surfaces. In DMD, discontinuous step functions of the interparticle distance were adopted and particles were moved at constant velocities between steps. Compared with conventional MD simulations,[96−100] our DMD simulation combining the merits of both DMD simulations and Go-like model achieves better efficiency while offering acceptable accuracy. More details about the simulation algorithm of DMD simulations with the Go-like model for protein adsorption can be found in the recent publication[87] from Zheng and Wei.

The systems were simulated in a box of 10.0 × 10.0 × 10.0 nm^3, and surfaces were all on the X−Z plane. Since DMD is event-driven and the solvent is represented only implicitly, it is not straightforward to correlate the simulation time and the temperature with the real time and temperature.[86] To address this issue, instead of applying the real units, we used time step t and reduced temperature $T^* = T/T_s$ in the simulations.[87] We assigned T_s = 503.2 K because we set $\mathcal{N}k_BT_s = E$, where k_B stands for Boltzmann's constant, $\mathcal{N}$ for Avogadro's number, and E for one unit of energy, taken to be 1 kcal/mol.[87] We chose T^* = 0.5 (approximately 250 K) because at such a temperature the SUP protein does not denature in the bulk water. A protein was initially placed above the surface with a gapping distance of ∼2.0 nm with negligible protein−surface interactions. As a protein reaches the surface's vicinity within a cutoff distance of 0.3 nm, a harmonic potential between the SAM surface and the residue's immobilization site was formed to mimic the grafting of a protein onto the SAM surface via site Cys 105.

The initial velocity of each atom was selected from the Maxwell−Boltzmann distribution at T = 0.4. After simulation with 5000 time steps, the system was stabilized. Then, the

https://doi.org/10.1021/acs.jpcb.1c03849
J. Phys. Chem. B 2021, 125, 7706−7716

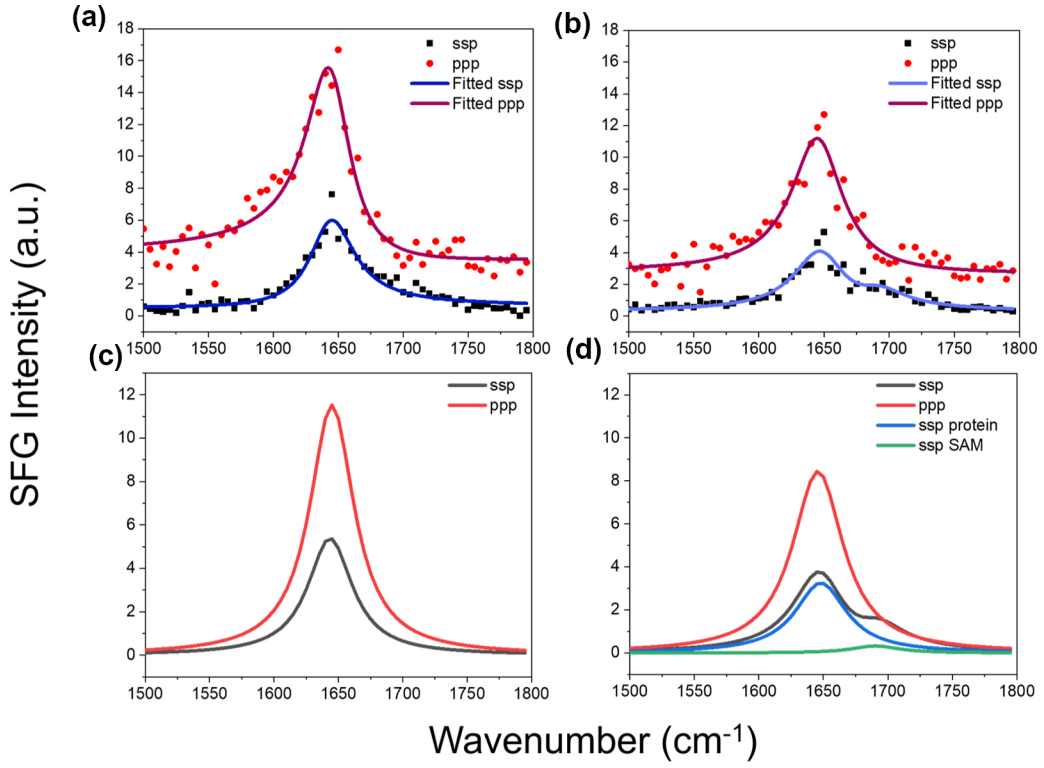

Figure 1. SFG ssp and ppp amide I spectra collected from the interfaces between surface-immobilized (a) SUP-C105 in contact with PB solution and (b) SUP-C105 in contact with a 100 μM uranyl ion PB solution. Dots represent experimental data, while lines are fitting curves. Fitted resonant SFG spectra from the immobilized (c) SUP-C105 in contact with PB solution and (d) SUP-C105 in contact with a 100 μM uranyl ion PB solution. Black: ssp spectra. Red: ppp spectra. The ssp spectra in (d) were divided into the SUP contribution (blue) and the SAM contribution (green, this fitted signal from SAM is very small). It is worth noting that no SFG signal can be detected from the SAM surface (before SUP immobilization) in the amide I signal frequency region.[38]

system was heated by a series of short runs that gradually increased T^* from 0.4 to 0.5, and during each run, we simulated for 20,000 time steps. DMD simulations were then carried out at 0.5 (approximately 250 K) for 1×10^7 time steps. Multiple independent simulations with different initial orientations and velocity profiles were carried out for each system to assess the effect of initial conditions. The initial orientations were randomly assigned.

RESULTS AND DISCUSSION

SFG ssp and ppp spectra were collected from immobilized SUP-C105 in contact with PB solution and with the same buffer containing 100 μM uranyl ions. These spectra, shown in Figure 1a,b, contain nonresonant signals. Therefore, to compare with calculated SFG spectra using the Hamiltonian approach which only have resonant contributions, these nonresonant contributions must be separated by spectral fitting to obtain spectra containing solely resonant signals, as shown in Figure 1c,d. Figure 1 shows that each ppp spectrum or ssp spectrum of immobilized SUP-C105 before uranyl ion binding only contains one peak, which is contributed by the SUP amide I mode. In contrast, the ssp SFG spectrum of SUP-C105 in the presence of a uranyl ion has two peaks. The small peak in the higher frequency region (centered at ~1700 cm^{-1}) is contributed by the SAM substrate. The interaction of the SAM carbonyl group with the immobilized SUP leads to the ordering of the SAM carbonyl group to contribute the SFG C═O stretching signal. The stronger peak is the amide I signal of surface-immobilized SUP, which was used for comparing with the spectra calculated using the Hamiltonian approach discussed below.

We have extensively studied the surface-immobilized protein orientation using our developed method with SFG spectra collected using different polarization combinations.[24,25,32−45] In order to determine the protein orientation with SFG spectra, in the past, we usually used the protein crystal structure to perform data analysis, assuming that the protein at the interface has a similar structure to those in crystals.[25,82,84] This assumption was tested by coarse-grained MD simulations.[89,90] Inspired by these previous studies, in this work, we first adopted the published SUP crystal structure PDB ID 4FZO as the input for the Hamiltonian program to simulate the SFG spectra to compare with the experimental SFG data to deduce the interfacial structures and orientations of surface-immobilized SUP-C105. DMD simulations were then conducted to examine the obtained interfacial structures and orientations. Based on the DMD results, although the final states of surface-immobilized SUP-C105 adopt lying-down representations, there are discrepancies in terms of conformations when compared with corresponding crystal structures. These structural differences would affect spatial coupling effects and alter the Hamiltonian calculation results. Therefore, to increase the accuracy of interfacial structural analysis, the DMD output structures were utilized as candidates for the Hamiltonian calculations to generate new orientation outcomes. With this same methodology, the SUP crystal structure PDB ID 4FZP was used for the data analysis of surface-immobilized SUP-C105 after uranyl ion binding. Because the difference between 4FZO and 4FZP is not

https://doi.org/10.1021/acs.jpcb.1c03849
J. Phys. Chem. B 2021, 125, 7706−7716

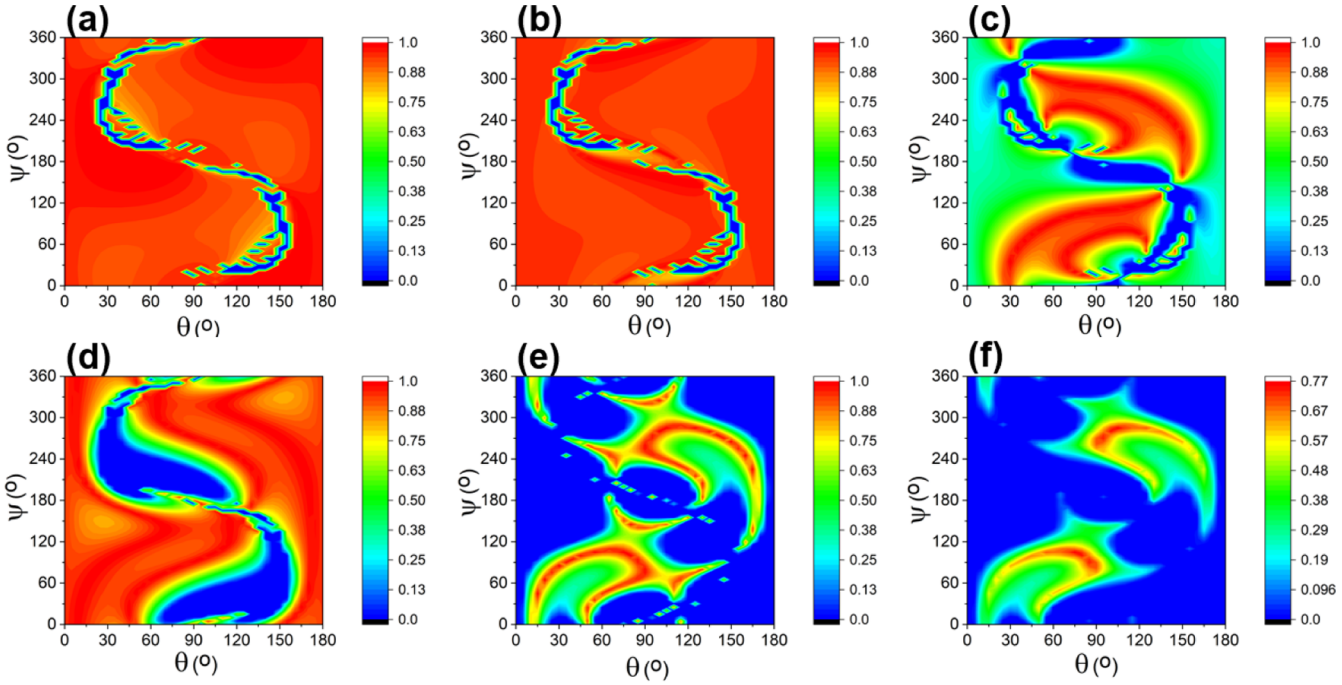

Figure 2. Heat maps of the matching scores between SFG spectra calculated by the Hamiltonian approach using 4FZO and experimentally collected SFG spectra of surface-immobilized SUP-C105 before uranyl ion binding based on (a) ppp peak center (score 1), (b) ssp peak center (score 2), (c) ppp peak width (score 3), (d) ssp peak width (score 4), and (e) $\chi^{(2)}_{zzz}/\chi^{(2)}_{yyz}$ (score 5). (f) Final score map of the multiplication of score 1 to 5.

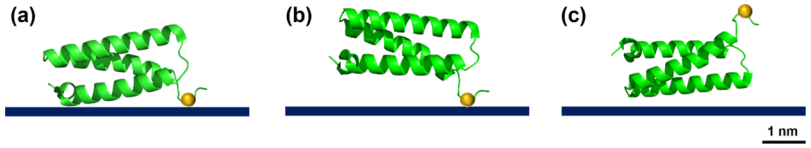

Figure 3. 4FZO orientation of (a) (0°, 0°), (b) (75°, 105°), and (c) (105°, 285°) after immobilization via Cys 105. The surface immobilization site (cysteine) is plotted in yellow. The calculated spectra are shown in the Supporting Information (Figure S5).

significant,[23,47] we assumed that the interfacial structures of surface-immobilized SUP-C105 before and after uranyl ion binding should also be similar. Therefore, the DMD results of the surface-immobilized SUP-C105 before uranyl ion binding can be adopted to approximate the structures of the protein after uranyl ion binding to improve the data analysis. We will first introduce our methodology by illustrating the process of determining conformation(s) and orientation(s) of surface-immobilized SUP-C105 before uranyl ion binding. This same strategy was applied to deduce conformations and orientations of the cases for SUP-C105 after binding to uranyl ion. Results will be compared and summarized in the last section.

First, the Hamiltonian approach was used to calculate the SFG spectra as a function of SUP orientation angles (θ, ψ) using 4FZO. Each spectrum (corresponding to each orientation) was then fitted to obtain five parameters: (a) ppp peak center (score 1), (b) ssp peak center (score 2), (c) ppp peak width (score 3), (d) ssp peak width (score 4), and (e) $\chi^{(2)}_{zzz}/\chi^{(2)}_{yyz}$ (score 5). These parameters were evaluated by the scoring system presented above to generate matching score maps. The five score maps with score 1 to score 5 based on the five matching criteria are shown in Figure 2, which quantify comparisons between the calculated SFG spectra of 4FZO and corresponding experimental spectra of surface-immobilized SUP-C105 before uranyl ion binding. By multiplying the scores of these five heat maps, a final score heat map considering all five matching criteria, also shown in Figure 2, is obtained to identify the most likely orientation(s) of the surface-immobilized protein. It is worth reiterating that in this study, the matching scores were generated by comparing the fitting parameters of the calculated and collected SFG spectra. We are developing methodology to compare the calculated spectra to the collected spectra point by point with the least linear square method to generate matching scores, which will be reported in the future.

It is worth noting that here the azimuthal angle average was applied when calculating the SFG spectra. Thus, the obtained final score map represents a symmetric feature: the score of (θ, ψ) is equal to the one of ($180° - \theta$, $180° + \psi$), which means that the absolute orientation (up or down) cannot be differentiated in the heat map. Therefore, the final score map always generates a pair of the most possible orientations. Here, the two most possible orientations of surface-immobilized SUP-C105 before uranyl ion binding by using 4FZO as the input structure are (75°, 105°), and (105°, 285°), visualized in Figure 3. The visualized structures clearly show that orientation (75°, 105°) has the immobilization cysteine site close to the surface, while orientation (105°, 285°) has the immobilization site diffused away from the surface. Thus, orientation (75°, 105°) should be the only most possible orientation of surface-immobilized SUP-C105 using 4FZO as an input structure, whose spectra are shown in Supporting

https://doi.org/10.1021/acs.jpcb.1c03849
J. Phys. Chem. B 2021, 125, 7706−7716

Information, S4. This deduced orientation shows a lying-down orientation of surface-immobilized SUP-C105 due to strong interactions between protein α helices and the SAM surface.

DMD simulations were performed to examine the deduced lying-down orientation of surface-immobilized SUP-C105. Four simulation runs were performed with different initial protein orientations and velocity profiles, leading to four final orientations (Figure 4). Figure 4 shows clearly that for case 1 to case 3, the SUP molecule lies down on the surface due to the strong SUP−surface interaction, consistent with our above SFG data analysis. In contrast, case 4 shows a standing posture for surface-immobilized SUP-C105; however, after the analysis below, this possibility can be ruled out. From careful comparison of the four orientations, we found that the tertiary structures of SUP vary slightly in different simulations. Therefore, to better resolve both the interfacial conformation and orientation of surface-immobilized SUP-C105, these protein structures obtained from DMD simulations were used as the Hamiltonian program inputs to re-calculate SUP orientation-dependent SFG spectra, and the obtained spectra were compared with experimental SFG data again to deduce surface-immobilized SUP-C105 orientation. Score maps generated from these new sets of comparisons are shown in Figure 5. The best matches for each of the four runs are DMD case 1 (40°, 90°), case 2 (55°, 75°), case 3 (50°, 280°) and case 4 (70°, 140°) (visualized in Figure 6). Although there are multiple matches, the matching structures of case 1 to case 3 are similar: the third helical chain (near C-terminus) is the closest to the surface, the middle helical chain is furthest from the surface, and the first helical chain is tilted with the N-terminus close to the surface (here, we define chain 1 as 6Ser−26Ser, chain 2 as 30Ser−53Lys, and chain 3 as 55Asp−76Leu based on the published SUP crystal structures 4FZO and 4FZP). We choose the case 2 orientation as the most likely orientation of surface-immobilized SUP-C105 because it has the highest matching scores among all four cases. In addition, we normalized these calculated spectra (using 4FZO and the DMD structures) and reconstructed experimental spectra to compare with each other (shown in Figure 7). Figure 7 shows that both ssp and ppp spectra of case 2 (55°, 75°) have the best overlaps with corresponding experimental spectra, which proves that case 2 (55°, 75°) is the best match among all the

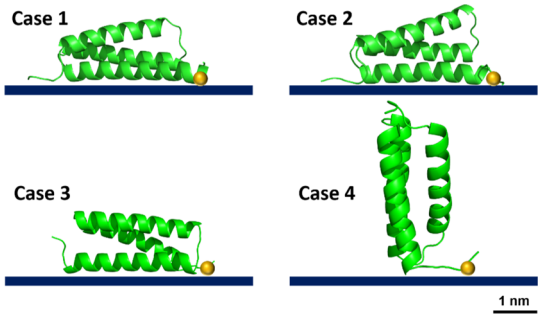

Figure 4. Simulated results of surface-immobilized SUP-C105 on the maleimide-terminated SAM surface using the DMD approach. The surface immobilization site (cysteine) is labeled as a yellow ball. Protein−surface interaction energies E_{ps} for the four cases are as follows: −26.27 kcal/mol (case 1), −27.89 kcal/mol (case 2), −18.95 kcal/mol (case 3), and −16.02 kcal/mol (case 4). Note: a negative value represents an attractive interaction energy and a positive value stands for a repulsion energy. The differences of chain−surface interaction energies are as follows: 14.23 kcal/mol for $\Delta E_{1,3} = E_{chain1} - E_{chain3}$ and 14.41 kcal/mol for $\Delta E_{2,3} = E_{chain2} - E_{chain3}$.

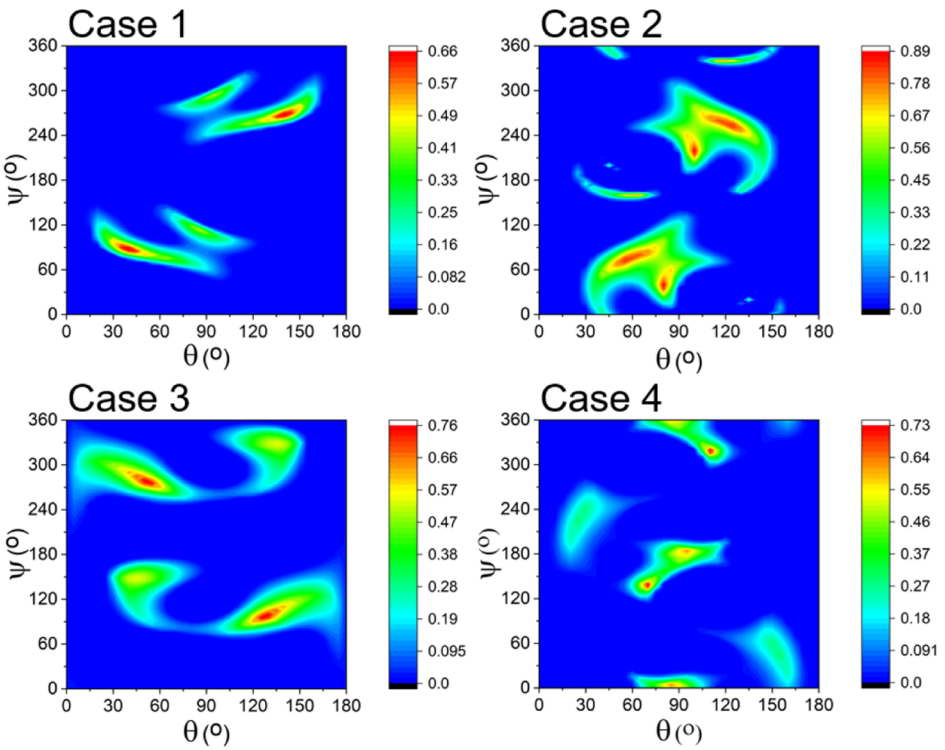

Figure 5. Final score map showing the matching scores between SFG experimental data and calculated spectra of DMD structures (case 1 to case 4) using the Hamiltonian approach as a function of orientation angles for immobilized SUP-C105 before uranyl ion binding based on all five matching criteria.

https://doi.org/10.1021/acs.jpcb.1c03849
J. Phys. Chem. B 2021, 125, 7706−7716

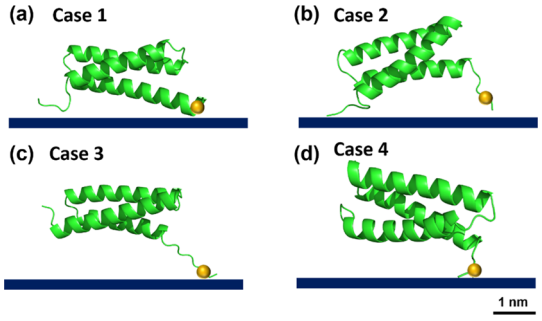

Figure 6. Visualized structures with the best matching scores with experimental data using DMD structures as inputs for the Hamiltonian approach calculation: (a) case 1 (40°, 90°), (b) case 2 (55°, 75°), (c) case 3 (50°, 280°), and (d) case 4 (70°, 140°) of surface-immobilized SUP-C105.

obtained matched orientations of surface-immobilized SUP-C105.

The hydrophobic residues of SUP are evenly distributed to allow all three helical chains to have hydrophobic interaction with the surface, and the immobilization site located near the C-terminus restricts the rotation of SUP to prevent the middle chain (the helical chain is not connected to the C- or N-terminus) from contacting the surface. In addition, the charged residues are mainly distributed on chain 1 (near N-terminus) and chain 2, which favors the interaction with the solvent molecules. Therefore, we hypothesize that chain 3 would have the highest affinity with a hydrophobic SAM surface, consistent with our matching results using DMD output structures. The matching result using a SUP crystal structure (4FZO), which shows chain 1 lying down to interact with the surface, failed to correlate with the above analysis. In theory, the final equilibrated DMD simulation structures shown in Figure 4 are well-calibrated, so the final orientation of the (0°, 0°) or [(0°, 180°) or (180°, 360°)] angle combination should be obtained from the SFG measurements as well, if the experimental data and simulation results match with each other perfectly. As we presented above, the DMD output structure case 4 shows a standing-up pose, in contrast to the other three cases. Here, the result obtained from the Hamiltonian calculation and experimental data matching indicates that SUP indeed adopts a lying-down pose, which is more reasonable. Although case 2 (55°, 75°) is not perfectly aligned with the DMD simulation and Hamiltonian input orientation (0°, 0°) numerically, the visualized structure of these two shows that the spatial arrangement of the three helical chains versus the surface plane is similar. The comparison of protein−surface interaction energies E_{ps} also shows that E_{ps} in case 2, where chain 3 is closest to the surface, is the strongest among all the four cases (Figure 4). Moreover, in case 2, chain 3 has more attractive interaction energy than the other two chains (Figure 4). Thus, combined with case 2 (55°, 75°) having the highest matching score leads us to conclude that it is the best match of surface-immobilized SUP-C105.

We adopted the same method to study SUP with a uranyl ion bound. By using SUP crystal structure 4FZP to calculate the SFG spectra of surface-immobilized SUP-C105 after uranyl ion binding with the Hamiltonian method, the best-matched protein orientation is determined to be (90°, 110°) (Supporting Information, S6), which is similar to the one (75°, 105°) of surface-immobilized SUP-C105 before uranyl ion binding (analyzed with 4FZO). This indicates that the interfacial structure of surface-immobilized SUP-C105 does not change substantially upon binding uranyl ions. Since uranyl ion binding has minor effects on the interfacial structure of surface SUP-C105, the above DMD results of surface-immobilized SUP-C105 before uranyl ion binding can be used as input structures of the Hamiltonian simulation program to calculate SFG spectra to match the experimental data obtained from surface-immobilized SUP-C105 after uranyl ion binding. With all four different SUP-C105 conformations obtained from the DMD simulation, the best matches are DMD case 1 (35°, 80°), case 2 (55°, 85°), case 3 (60°, 285°), and case 4 (25°, 250°) (Supporting Information, S7). Excluding case 4 (25°, 250°), the other three cases all present a lying-down configuration similar to those of surface-immobilized SUP-C105 before uranyl ion binding. Among all four cases after uranyl ion binding, the highest matching score is case 2 (55°, 85°), which also shows the best spectral match compared to other matched spectra (shown in Supporting Information, S7). We chose this case 2 orientation as the most likely orientation of the protein after binding to a uranyl ion. The above results regarding the SUP-C105 orientations show that before and after uranyl ion binding, the conformation remains the same (both for case 2) and the orientation changes slightly from (55°, 75°) to (55°, 85°). It is interesting to see that the matching scores for orientations of both surface-immobilized SUP-C105 before and after uranyl ion binding deduced using the DMD results are higher than those based on the crystal structures. This indicates that the interfacial

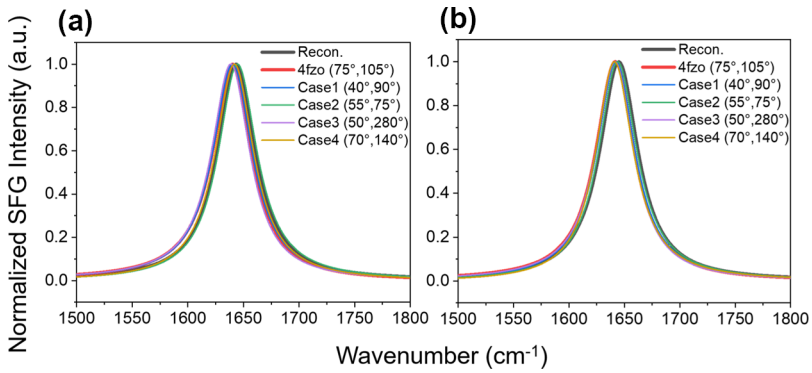

Figure 7. Spectral comparisons of (a) ssp and (b) ppp SFG spectra between the experimental reconstructed spectra of SUP-C105 before uranyl ion binding and best-matched calculated spectra using 4FZO and DMD-optimized structures without uranyl ion binding.

https://doi.org/10.1021/acs.jpcb.1c03849
J. Phys. Chem. B 2021, 125, 7706−7716

interaction leads to the SUP conformational change from its crystal structure.

Replotting all the obtained orientations in Figure 8, one can find that the best-matched results of SUP-C105 using 4FZO and 4FZP in the Hamiltonian calculation above both show that only chain 1 in SUP predominantly interacts with the SAM surface. However, the best-matched results of immobilized SUP-C105 using the DMD results show that chain 3 predominantly interacts with the surface. We believe that the matched DMD results are more reasonable because chain 3 contains the immobilization site (thereby restricting its motion), the highest content of hydrophobic residues to interact with the surface, and the least charged residues to interact with the solvent. DMD case 4 of SUP-C105, which shows a standing-up pose, is not a reliable interfacial structure of SUP-C105 for two reasons. First, the interaction between the SUP and the SAM surface is strong enough to prevent the protein from standing up based on the results obtained above. Second, the best match of surface-immobilized SUP-C105 before uranyl ion binding using case 4 generates an orientation unlike its original one, which failed to correlate DMD simulation and the Hamiltonian calculation.

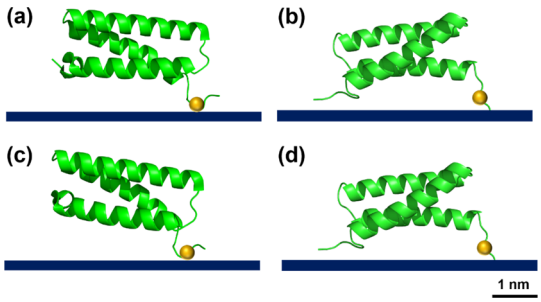

Figure 8. Schematics of the SUP-C105 orientation: (a) surface-immobilized SUP-C105 before uranyl ion binding deduced based on the crystal structure and (b) DMD results and (c) surface-immobilized SUP-C105 after uranyl ion binding deduced based on the crystal structure and (d) DMD results.

Previously, circular dichroism (CD) spectroscopy was used to investigate changes in the SUP secondary structure upon uranyl ion binding in solution. It was found that after adding 1 equiv uranyl ion to the SUP solution, the CD spectrum of the SUP molecules noticeably changed, with a loss of the 208 nm characteristic α helix band, implying that SUP changed its conformation or secondary structure dramatically after binding with uranyl ions in the solution state.[47] On the contrary, published crystal structures show that the SUP secondary structure is similar before and after uranyl ion binding.[23] Combined with the SFG and DMD simulation data discussed above, it can be concluded that the structural changes of the surface-immobilized SUP-C105 before and after uranyl ion binding are very small, with no conformational change and only a slight change in orientation. This conclusion is different from the case in free solution and similar to the conclusions reached from crystallography. This is reasonable because the surface-immobilized proteins have much less freedom compared to the proteins in free solution due to strong surface−protein interactions, similar to the constrained state of crystallized protein molecules. Here, our results show that the surface-immobilized SUP-C105 was lying down to a similar extent with or without the presence of uranyl ions (before or after uranyl ion binding) due to the strong restriction and hydrophobic interaction created by the SAM surface.

CONCLUSIONS

In this study, we successfully applied SFG spectroscopy, DMD simulation, and Hamiltonian approach for SFG spectra analysis together to study the structure and orientation of SUP immobilized on the SAM surface via immobilization site Cys 105. We summarized the process we used in this study into a flow chart in Supporting Information, Figure S10.

Because of the strong hydrophobic interactions between SUP and the SAM surface, immobilized SUP-C105 adopts a lying-down orientation. The orientation of the surface-immobilized SUP varies slightly upon uranyl ion binding, but the effects are not substantial. This is in contrast to the effect of uranyl ion binding on free SUP in solution (where large secondary structure changes were observed) and is similar to that of the crystal structures of SUP before and after uranyl ion binding (where there is almost no change). This research suggests that by using a less hydrophobic surface for SUP immobilization or by mutating some hydrophobic amino acids of SUP with hydrophilic ones (such amino acids should be far away from the binding domain so that the mutation would not interfere with the uranyl ion binding), the SUP−surface hydrophobic interaction should be reduced, which may favor a standing-up pose of the SUP to better expose uranyl ion binding sites.

ASSOCIATED CONTENT

Supporting Information

The Supporting Information is available free of charge at https://pubs.acs.org/doi/10.1021/acs.jpcb.1c03849.

Details about the matching heat maps, SFG spectra fitting parameters, heat maps for all the simulated structures, and Hamiltonian calculation (PDF)

AUTHOR INFORMATION

Corresponding Authors

Tao Wei − *Department of Chemical Engineering, Howard University, Washington, D.C. 20059, United States;* orcid.org/0000-0001-6888-1658; Email: tao.wei@howard.edu

E. Neil G. Marsh − *Department of Chemistry, University of Michigan, Ann Arbor, Michigan 48109, United States;* orcid.org/0000-0003-1713-1683; Email: nmarsh@umich.edu

Zhan Chen − *Department of Chemistry, University of Michigan, Ann Arbor, Michigan 48109, United States;* orcid.org/0000-0001-8687-8348; Email: zhanc@umich.edu

Authors

Wen Guo − *Department of Chemistry, University of Michigan, Ann Arbor, Michigan 48109, United States*

Xingquan Zou − *Department of Chemistry, University of Michigan, Ann Arbor, Michigan 48109, United States;* orcid.org/0000-0002-9716-9771

Hanjie Jiang − *Department of Chemistry, University of Michigan, Ann Arbor, Michigan 48109, United States*

Karl J. Koebke − *Department of Chemistry, University of Michigan, Ann Arbor, Michigan 48109, United States;* orcid.org/0000-0003-2198-2667

https://doi.org/10.1021/acs.jpcb.1c03849
J. Phys. Chem. B 2021, 125, 7706−7716

Marie Hoarau − *Department of Chemistry, University of Michigan, Ann Arbor, Michigan 48109, United States*
Ralph Crisci − *Department of Chemistry, University of Michigan, Ann Arbor, Michigan 48109, United States*
Tieyi Lu − *Department of Chemistry, University of Michigan, Ann Arbor, Michigan 48109, United States*

Complete contact information is available at: https://pubs.acs.org/10.1021/acs.jpcb.1c03849

Notes

The authors declare no competing financial interest.

■ ACKNOWLEDGMENTS

This research was supported by the Defense Threat Reduction Agency (HDTRA1-16-1-0004). Z.C. also thanks the support from the National Science Foundation (CHE-1904380) for the development/application of the Hamiltonian calculation of interfacial biomolecules. T.W. thanks the support from the Office of Naval Research (N00014-20-1-2215) for DMD simulations. E.N.G.M. acknowledges support from the National Science Foundation (CHE -1904759) and the Army Research Office (W911NF-20-1-0150).

■ REFERENCES

(1) Moutsiopoulou, A.; Broyles, D.; Joda, H.; Dikici, E.; Kaur, A.; Kaifer, A.; Daunert, S.; Deo, S. K. Bioluminescent Protein−Inhibitor Pair in the Design of a Molecular Aptamer Beacon Biosensing System. *Anal. Chem.* **2020**, *92*, 7393−7398.
(2) Okkelman, I. A.; McGarrigle, R.; O'Carroll, S.; Berrio, D. C.; Schenke-Layland, K.; Hynes, J.; Dmitriev, R. I. Extracellular Ca^{2+}-Sensing Fluorescent Protein Biosensor Based on a Collagen-Binding Domain. *ACS Appl. Bio Mater.* **2020**, *3*, 5310−5321.
(3) Białek, R.; Thakur, K.; Ruff, A.; Jones, M. R.; Schuhmann, W.; Ramanan, C.; Gibasiewicz, K. Insight into Electron Transfer from a Redox Polymer to a Photoactive Protein. *J. Phys. Chem. B* **2020**, *124*, 11123−11132.
(4) Zander, N. E.; Orlicki, J. A.; Rawlett, A. M.; Beebe, T. P. Quantification of Protein Incorporated into Electrospun Polycaprolactone Tissue Engineering Scaffolds. *ACS Appl. Mater. Interfaces* **2012**, *4*, 2074−2081.
(5) Tsang, T. F.; Qiu, Y.; Lin, L.; Ye, J.; Ma, C.; Yang, X. Simple Method for Studying *in Vitro* Protein−Protein Interactions Based on Protein Complementation and Its Application in Drug Screening Targeting Bacterial Transcription. *ACS Infect. Dis.* **2019**, *5*, 521−527.
(6) Iida, S.; Nakamura, H. K.; Mashimo, T.; Fukunishi, Y. Structural Fluctuations of Aromatic Residues in an Apo-Form Reveal Cryptic Binding Sites: Implications for Fragment-Based Drug Design. *J. Phys. Chem. B* **2020**, *124*, 9977−9986.
(7) Rajagopal, N.; Irudayanathan, F. J.; Nangia, S. Palmitoylation of Claudin-5 Proteins Influences Their Lipid Domain Affinity and Tight Junction Assembly at the Blood−Brain Barrier Interface. *J. Phys. Chem. B* **2019**, *123*, 983−993.
(8) Yu, B.; Pletka, C. C.; Iwahara, J. NMR Observation of Intermolecular Hydrogen Bonds between Protein Tyrosine Side-Chain OH and DNA Phosphate Groups. *J. Phys. Chem. B* **2020**, *124*, 1065−1070.
(9) Girvin, Z. C.; Gellman, S. H. Foldamer Catalysis. *J. Am. Chem. Soc.* **2020**, *142*, 17211−17223.
(10) Antoniou, D.; Schwartz, S. D. Role of Protein Motions in Catalysis by Formate Dehydrogenase. *J. Phys. Chem. B* **2020**, *124*, 9483−9489.
(11) Nivens, D. A.; Zhang, Y.; Angel, S. M. Detection of Uranyl Ion via Fluorescence Quenching and Photochemical Oxidation of Calcein. *J. Photochem. Photobiol., A* **2002**, *152*, 167−173.
(12) Murty, B. Spectrophotometric Determination of Uranium in Process Streams of a Uranium Extraction Plant. *Talanta* **1997**, *44*, 283−295.
(13) Ghaedi, M.; Tashkhourian, J.; Montazerozohori, M.; Pebdani, A. A.; Khodadoust, S. Design of an Efficient Uranyl Ion Optical Sensor Based on 1′-2,2′-(1,2-Phenylene)Bis(Ethene-2,1-Diyl)-Dinaphthalen-2-Ol. *Mater. Sci. Eng., C* **2012**, *32*, 1888−1892.
(14) Lu, G.; Forbes, T. Z.; Haes, A. J. Evaluating Best Practices in Raman Spectral Analysis for Uranium Speciation and Relative Abundance in Aqueous Solutions. *Anal. Chem.* **2016**, *88*, 773−780.
(15) Lu, G.; Johns, A. J.; Neupane, B.; Phan, H. T.; Cwiertny, D. M.; Forbes, T. Z.; Haes, A. J. Matrix-Independent Surface-Enhanced Raman Scattering Detection of Uranyl Using Electrospun Amidoximated Polyacrylonitrile Mats and Gold Nanostars. *Anal. Chem.* **2018**, *90*, 6766−6772.
(16) Savina, M. R.; Isselhardt, B. H.; Kucher, A.; Trappitsch, R.; King, B. V.; Ruddle, D.; Gopal, R.; Hutcheon, I. High Useful Yield and Isotopic Analysis of Uranium by Resonance Ionization Mass Spectrometry. *Anal. Chem.* **2017**, *89*, 6224−6231.
(17) Hodisan, T.; Curtui, M.; Cobzac, S.; Cimpoiu, C.; Haiduc, I. The Limit of Detection Improvement in TLC Determination of Uranium and Thorium in the Presence of Other Metal Ions. *J. Radioanal. Nucl. Chem.* **1998**, *238*, 179−183.
(18) Peled, Y.; Krent, E.; Tal, N.; Tobias, H.; Mandler, D. Electrochemical Determination of Low Levels of Uranyl by a Vibrating Gold Microelectrode. *Anal. Chem.* **2015**, *87*, 768−776.
(19) Becker, A.; Tobias, H.; Mandler, D. Electrochemical Determination of Uranyl Ions Using a Self-Assembled Monolayer. *Anal. Chem.* **2009**, *81*, 8627−8631.
(20) Ghoreishi, S. M.; Behpour, M.; Mazaheri, S.; Naeimi, H. Uranyl Sensor Based on a N,N′-Bis(Salicylidene)-2-Hydroxy-Phenylmethanediamine and Multiwall Carbon Nanotube Electrode. *J. Radioanal. Nucl. Chem.* **2012**, *293*, 201−210.
(21) Meir, R.; Zverzhinetsky, M.; Harpak, N.; Borberg, E.; Burstein, L.; Zeiri, O.; Krivitsky, V.; Patolsky, F. Direct Detection of Uranyl in Urine by Dissociation from Aptamer-Modified Nanosensor Arrays. *Anal. Chem.* **2020**, *92*, 12528−12537.
(22) Feng, M.; Gu, C.; Sun, Y.; Zhang, S.; Tong, A.; Xiang, Y. Enhancing Catalytic Activity of Uranyl-Dependent DNAzyme by Flexible Linker Insertion for More Sensitive Detection of Uranyl Ion. *Anal. Chem.* **2019**, *91*, 6608−6615.
(23) Zhou, L.; Bosscher, M.; Zhang, C.; Özçubukçu, S.; Zhang, L.; Zhang, W.; Li, C. J.; Liu, J.; Jensen, M. P.; Lai, L.; et al. A Protein Engineered to Bind Uranyl Selectively and with Femtomolar Affinity. *Nat. Chem.* **2014**, *6*, 236−241.
(24) Hoarau, M.; Badieyan, S.; Marsh, E. N. G. Immobilized Enzymes: Understanding Enzyme−Surface Interactions at the Molecular Level. *Org. Biomol. Chem.* **2017**, *15*, 9539−9551.
(25) Liu, Y.; Ogorzalek, T. L.; Yang, P.; Schroeder, M. M.; Marsh, E. N. G.; Chen, Z. Molecular Orientation of Enzymes Attached to Surfaces through Defined Chemical Linkages at the Solid−Liquid Interface. *J. Am. Chem. Soc.* **2013**, *135*, 12660−12669.
(26) Sassolas, A.; Blum, L. J.; Leca-Bouvier, B. D. Immobilization Strategies to Develop Enzymatic Biosensors. *Biotechnol. Adv.* **2012**, *30*, 489−511.
(27) Brady, D.; Jordaan, J. Advances in Enzyme Immobilisation. *Biotechnol. Lett.* **2009**, *31*, 1639−1650.
(28) Samajdar, R. N.; Kumar, C.; Viswanath, P.; Bhattacharyya, A. J. Studying Hemoglobin and a Bare Metal−Porphyrin Complex Immobilized on Functionalized Silicon Surfaces Using Synchrotron X-Ray Reflectivity. *J. Phys. Chem. B* **2019**, *123*, 7492−7503.
(29) Sáringer, S.; Akula, R. A.; Szerlauth, A.; Szilagyi, I. Papain Adsorption on Latex Particles: Charging, Aggregation, and Enzymatic Activity. *J. Phys. Chem. B* **2019**, *123*, 9984−9991.
(30) Tuan Kob, T. N. A.; Ismail, M. F.; Abdul Rahman, M. B.; Cordova, K. E.; Mohammad Latif, M. A. Unraveling the Structural Dynamics of an Enzyme Encapsulated within a Metal−Organic Framework. *J. Phys. Chem. B* **2020**, *124*, 3678−3685.

(31) Chin, M.; Tada, S.; Tsai, M.-H.; Ito, Y.; Luo, S.-C. Strategy to Immobilize Peptide Probe Selected through In Vitro Ribosome Display for Electrochemical Aptasensor Application. *Anal. Chem.* **2020**, *92*, 11260−11267.
(32) Ye, S.; Nguyen, K. T.; Boughton, A. P.; Mello, C. M.; Chen, Z. Orientation Difference of Chemically Immobilized and Physically Adsorbed Biological Molecules on Polymers Detected at the Solid/Liquid Interfaces in Situ. *Langmuir* **2010**, *26*, 6471−6477.
(33) Han, X.; Soblosky, L.; Slutsky, M.; Mello, C. M.; Chen, Z. Solvent Effect and Time-Dependent Behavior of C-Terminus-Cysteine-Modified Cecropin P1 Chemically Immobilized on a Polymer Surface. *Langmuir* **2011**, *27*, 7042−7051.
(34) Han, X.; Liu, Y.; Wu, F.-G.; Jansensky, J.; Kim, T.; Wang, Z.; Brooks, C. L.; Wu, J.; Xi, C.; Mello, C. M.; et al. Different Interfacial Behaviors of Peptides Chemically Immobilized on Surfaces with Different Linker Lengths and via Different Termini. *J. Phys. Chem. B* **2014**, *118*, 2904−2912.
(35) Shen, L.; Schroeder, M.; Ogorzalek, T. L.; Yang, P.; Wu, F.-G.; Marsh, E. N. G.; Chen, Z. Surface Orientation Control of Site-Specifically Immobilized Nitro-reductase (NfsB). *Langmuir* **2014**, *30*, 5930−5938.
(36) Shen, L.; Ulrich, N. W.; Mello, C. M.; Chen, Z. Determination of conformation and orientation of immobilized peptides and proteins at buried interfaces. *Chem. Phys. Lett.* **2015**, *619*, 247−255.
(37) Ogorzalek, T. L.; Wei, S.; Liu, Y.; Wang, Q.; Brooks, C. L.; Chen, Z.; Marsh, E. N. G. Molecular-Level Insights into Orientation-Dependent Changes in the Thermal Stability of Enzymes Covalently Immobilized on Surfaces. *Langmuir* **2015**, *31*, 6145−6153.
(38) Wang, Q.; Wei, S.; Wu, J.; Zou, X.; Sieggreen, O.; Liu, Y.; Xi, C.; Brooks, C. L.; Chen, Z. Interfacial Behaviors of Antimicrobial Peptide Cecropin P1 Immobilized on Different Self-Assembled Monolayers. *J. Phys. Chem. C* **2015**, *119*, 22542−22551.
(39) Badieyan, S.; Wang, Q.; Zou, X.; Li, Y.; Herron, M.; Abbott, N. L.; Chen, Z.; Marsh, E. N. G. Engineered Surface-Immobilized Enzyme That Retains High Levels of Catalytic Activity in Air. *J. Am. Chem. Soc.* **2017**, *139*, 2872−2875.
(40) Xiao, M.; Jasensky, J.; Gerszberg, J.; Chen, J.; Tian, J.; Lin, T.; Lu, T.; Lahann, J.; Chen, Z. Chemically Immobilized Antimicrobial Peptide on Polymer and Self-Assembled Monolayer Substrates. *Langmuir* **2018**, *34*, 12889−12896.
(41) Jasensky, J.; Ferguson, K.; Baria, M.; Zou, X.; McGinnis, R.; Kaneshiro, A.; Badieyan, S.; Wei, S.; Marsh, E. N. G.; Chen, Z. Simultaneous Observation of the Orientation and Activity of Surface-Immobilized Enzymes. *Langmuir* **2018**, *34*, 9133−9140.
(42) Zou, X.; Wei, S.; Badieyan, S.; Schroeder, M.; Jasensky, J.; Brooks, C. L.; Marsh, E. N. G.; Chen, Z. Investigating the Effect of Two-Point Surface Attachment on Enzyme Stability and Activity. *J. Am. Chem. Soc.* **2018**, *140*, 16560−16569.
(43) Ding, B.; Jasensky, J.; Li, Y.; Chen, Z. Engineering and Characterization of Peptides and Proteins at Surfaces and Interfaces: A Case Study in Surface-Sensitive Vibrational Spectroscopy. *Acc. Chem. Res.* **2016**, *49*, 1149−1157.
(44) Li, Y.; Ogorzalek, T. L.; Wei, S.; Zhang, X.; Yang, P.; Jasensky, J.; Brooks, C. L.; Marsh, E. N. G.; Chen, Z. Effect of Immobilization Site on the Orientation and Activity of Surface-Tethered Enzymes. *Phys. Chem. Chem. Phys.* **2018**, *20*, 1021−1029.
(45) Wang, Z.; Han, X.; He, N.; Chen, Z.; Brooks, C. L. Molecular Structures of C- and N-Terminus Cysteine Modified Cecropin P1 Chemically Immobilized onto Maleimide-Terminated Self-Assembled Monolayers Investigated by Molecular Dynamics Simulation. *J. Phys. Chem. B* **2014**, *118*, 5670−5680.
(46) Hosseinpour, S.; Roeters, S. J.; Bonn, M.; Peukert, W.; Woutersen, S.; Weidner, T. Structure and Dynamics of Interfacial Peptides and Proteins from Vibrational Sum-Frequency Generation Spectroscopy. *Chem. Rev.* **2020**, *120*, 3420−3465.
(47) Hoarau, M.; Koebke, K. J.; Chen, Z.; Marsh, E. N. G. Probing Metal Ion Discrimination in a Protein Designed to Bind Uranyl Cation With Femtomolar Affinity. *Front. Mol. Biosci.* **2019**, *6*, 73.
(48) Shen, Y. R. Phase-Sensitive Sum-Frequency Spectroscopy. *Annu. Rev. Phys. Chem.* **2013**, *64*, 129−150.
(49) Gracias, D. H.; Chen, Z.; Shen, Y. R.; Somorjai, G. A. Molecular Characterization of Polymer and Polymer Blend Surfaces. Combined Sum Frequency Generation Surface Vibrational Spectroscopy and Scanning Force Microscopy Studies. *Acc. Chem. Res.* **1999**, *32*, 930−940.
(50) Inoue, K.-i.; Takada, C.; Wang, L.; Morita, A.; Ye, S. *In Situ* Monitoring of the Unsaturated Phospholipid Monolayer Oxidation in Ambient Air by HD-SFG Spectroscopy. *J. Phys. Chem. B* **2020**, *124*, 5246−5250.
(51) Wang, Z.; Fu, L.; Yan, E. C. Y. C−H Stretch for Probing Kinetics of Self-Assembly into Macromolecular Chiral Structures at Interfaces by Chiral Sum Frequency Generation Spectroscopy. *Langmuir* **2013**, *29*, 4077−4083.
(52) Makarem, M.; Nishiyama, Y.; Xin, X.; Durachko, D. M.; Gu, Y.; Cosgrove, D. J.; Kim, S. H. Distinguishing Mesoscale Polar Order (Unidirectional vs Bidirectional) of Cellulose Microfibrils in Plant Cell Walls Using Sum Frequency Generation Spectroscopy. *J. Phys. Chem. B* **2020**, *124*, 8071−8081.
(53) Malyk, S.; Shalhout, F. Y.; O'Leary, L. E.; Lewis, N. S.; Benderskii, A. V. Vibrational Sum Frequency Spectroscopic Investigation of the Azimuthal Anisotropy and Rotational Dynamics of Methyl-Terminated Silicon(111) Surfaces. *J. Phys. Chem. C* **2013**, *117*, 935−944.
(54) Li, Q.; Hua, R.; Cheah, I. J.; Chou, K. C. Surface Structure Relaxation of Poly(Methyl Methacrylate). *J. Phys. Chem. B* **2008**, *112*, 694−697.
(55) Perry, A.; Neipert, C.; Space, B.; Moore, P. B. Theoretical Modeling of Interface Specific Vibrational Spectroscopy: Methods and Applications to Aqueous Interfaces. *Chem. Rev.* **2006**, *106*, 1234−1258.
(56) Voegtle, M. J.; Pal, T.; Pennathur, A. K.; Menachekanian, S.; Patrow, J. G.; Sarkar, S.; Cui, Q.; Dawlaty, J. M. Interfacial Polarization and Ionic Structure at the Ionic Liquid−Metal Interface Studied by Vibrational Spectroscopy and Molecular Dynamics Simulations. *J. Phys. Chem. B* **2021**, *125*, 2741−2753.
(57) Wang, F.; Li, X.; Zhang, F.; Liu, X.; Hu, P.; Beke-Somfai, T.; Lu, X. Revealing Interfacial Lipid Hydrolysis Catalyzed by Phospholipase A_1 at Molecular Level via Sum Frequency Generation Vibrational Spectroscopy and Fluorescence Microscopy. *Langmuir* **2019**, *35*, 12831−12838.
(58) Richmond, G. L. Molecular Bonding and Interactions at Aqueous Surfaces as Probed by Vibrational Sum Frequency Spectroscopy. *Chem. Rev.* **2002**, *102*, 2693−2724.
(59) Chen, Z.; Shen, Y. R.; Somorjai, G. A. Studies of Polymer Surfaces by Sum Frequency Generation Vibrational Spectroscopy. *Annu. Rev. Phys. Chem.* **2002**, *53*, 437−465.
(60) Lu, X.; Zhang, C.; Ulrich, N.; Xiao, M.; Ma, Y.-H.; Chen, Z. Studying Polymer Surfaces and Interfaces with Sum Frequency Generation Vibrational Spectroscopy. *Anal. Chem.* **2017**, *89*, 466−489.
(61) Li, X.; Ma, L.; Lu, X. Calcium Ions Affect Water Molecular Structures Surrounding an Oligonucleotide Duplex as Revealed by Sum Frequency Generation Vibrational Spectroscopy. *Langmuir* **2018**, *34*, 14774−14779.
(62) Han, X.; Leng, C.; Shao, Q.; Jiang, S.; Chen, Z. Absolute Orientations of Water Molecules at Zwitterionic Polymer Interfaces and Interfacial Dynamics after Salt Exposure. *Langmuir* **2019**, *35*, 1327−1334.
(63) Xiao, M.; Mohler, C.; Tucker, C.; Walther, B.; Lu, X.; Chen, Z. Structures and Adhesion Properties at Polyethylene/Silica and Polyethylene/Nylon Interfaces. *Langmuir* **2018**, *34*, 6194−6204.
(64) Xiao, M.; Jasensky, J.; Foster, L.; Kuroda, K.; Chen, Z. Monitoring Antimicrobial Mechanisms of Surface-Immobilized Peptides in Situ. *Langmuir* **2018**, *34*, 2057−2062.
(65) Han, X.; Zheng, J.; Lin, F.; Kuroda, K.; Chen, Z. Interactions between Surface-Immobilized Antimicrobial Peptides and Model Bacterial Cell Membranes. *Langmuir* **2018**, *34*, 512−520.

https://doi.org/10.1021/acs.jpcb.1c03849
J. Phys. Chem. B 2021, 125, 7706−7716

(66) Hung, K.-K.; Stege, U.; Hore, D. K. IR Absorption, Raman Scattering, and IR-Vis Sum-Frequency Generation Spectroscopy as Quantitative Probes of Surface Structure. *Appl. Spectrosc. Rev.* **2015**, *50*, 351−376.
(67) Leng, C.; Hung, H.-C.; Sun, S.; Wang, D.; Li, Y.; Jiang, S.; Chen, Z. Probing the Surface Hydration of Nonfouling Zwitterionic and PEG Materials in Contact with Proteins. *ACS Appl. Mater. Interfaces* **2015**, *7*, 16881−16888.
(68) Wang, J.; Chen, X.; Clarke, M. L.; Chen, Z. Vibrational Spectroscopic Studies on Fibrinogen Adsorption at Polystyrene/Protein Solution Interfaces: Hydrophobic Side Chain and Secondary Structure Changes. *J. Phys. Chem. B* **2006**, *110*, 5017−5024.
(69) Nguyen, K. T.; Le Clair, S. V.; Ye, S.; Chen, Z. Molecular Interactions between Magainin 2 and Model Membranes in Situ. *J. Phys. Chem. B* **2009**, *113*, 12358−12363.
(70) von Domaros, M.; Liu, Y.; Butman, J. L.; Perlt, E.; Geiger, F. M.; Tobias, D. J. Molecular Orientation at the Squalene/Air Interface from Sum Frequency Generation Spectroscopy and Atomistic Modeling. *J. Phys. Chem. B* **2021**, *125*, 3932−3941.
(71) Ding, B.; Soblosky, L.; Nguyen, K.; Geng, J.; Yu, X.; Ramamoorthy, A.; Chen, Z. Physiologically-Relevant Modes of Membrane Interactions by the Human Antimicrobial Peptide, LL-37, Revealed by SFG Experiments. *Sci. Rep.* **2013**, *3*, 1854.
(72) Ding, B.; Panahi, A.; Ho, J.-J.; Laaser, J. E.; Brooks, C. L.; Zanni, M. T.; Chen, Z. Probing Site-Specific Structural Information of Peptides at Model Membrane Interface In Situ. *J. Am. Chem. Soc.* **2015**, *137*, 10190−10198.
(73) Premadasa, U. I.; Moradighadi, N.; Kotturi, K.; Nonkumwong, J.; Khan, M. R.; Singer, M.; Masson, E.; Cimatu, K. L. A. Solvent Isotopic Effects on a Surfactant Headgroup at the Air−Liquid Interface. *J. Phys. Chem. C* **2018**, *122*, 16079−16085.
(74) Perry, A.; Neipert, C.; Kasprzyk, C. R.; Green, T.; Space, B.; Moore, P. B. A Theoretical Description of the Polarization Dependence of the Sum Frequency Generation Spectroscopy of the Water/Vapor Interface. *J. Chem. Phys.* **2005**, *123*, 144705.
(75) Hall, S. A.; Jena, K. C.; Covert, P. A.; Roy, S.; Trudeau, T. G.; Hore, D. K. Molecular-Level Surface Structure from Nonlinear Vibrational Spectroscopy Combined with Simulations. *J. Phys. Chem. B* **2014**, *118*, 5617−5636.
(76) Krause, K. D.; Roy, S.; Hore, D. K. Interplay between Adsorbed Peptide Structure, Trapped Water, and Surface Hydrophobicity. *Biointerphases* **2017**, *12*, 02D407.
(77) Li, B.; Andre, J. S.; Chen, X.; Walther, B.; Paradkar, R.; Feng, C.; Tucker, C.; Mohler, C.; Chen, Z. Observing a Chemical Reaction at a Buried Solid/Solid Interface in Situ. *Anal. Chem.* **2020**, *92*, 14145−14152.
(78) Xiao, M.; Lu, T.; Lin, T.; Andre, J. S.; Chen, Z. Understanding Molecular Structures of Buried Interfaces in Halide Perovskite Photovoltaic Devices Nondestructively with Sub-monolayer Sensitivity using Sum Frequency Generation Vibrational Spectroscopy. *Adv. Energy Mater.* **2020**, *10*, 1903053.
(79) Chen, X.; Wang, J.; Sniadecki, J. J.; Even, M. A.; Chen, Z. Probing α-Helical and β-Sheet Structures of Peptides at Solid/Liquid Interfaces with SFG. *Langmuir* **2005**, *21*, 2662−2664.
(80) Nguyen, K. T.; Le Clair, S. V.; Ye, S.; Chen, Z. Orientation Determination of Protein Helical Secondary Structures Using Linear and Nonlinear Vibrational Spectroscopy. *J. Phys. Chem. B* **2009**, *113*, 12169−12180.
(81) Nguyen, K. T.; King, J. T.; Chen, Z. Orientation Determination of Interfacial β-Sheet Structures in Situ. *J. Phys. Chem. B* **2010**, *114*, 8291−8300.
(82) Boughton, A. P.; Yang, P.; Tesmer, V. M.; Ding, B.; Tesmer, J. J. G.; Chen, Z. Heterotrimeric G Protein B1γ2 Subunits Change Orientation upon Complex Formation with G Protein- Coupled Receptor Kinase 2 (GRK2) on a Model Membrane. *Proc. Natl. Acad. Sci. U.S.A.* **2011**, *108*, E667−E673.
(83) Zou, X.; Wei, S.; Jasensky, J.; Xiao, M.; Wang, Q.; Brooks, C. L., III; Chen, Z. Molecular Interactions between Graphene and Biological Molecules. *J. Am. Chem. Soc.* **2017**, *139*, 1928−1936.
(84) Yang, P.; Boughton, A.; Homan, K.; Tesmer, J.; Chen, Z. Membrane Orientation of Gα i β 1 γ 2 and Gβ 1 γ 2 Determined via Combined Vibrational Spectroscopic Studies. *J. Am. Chem. Soc.* **2013**, *135*, 5044−5051.
(85) Hamm, P.; Zanni, M. *Concepts and Methods of 2D Infrared Spectroscopy*; Cambridge University Press: Cambridge, UK, 2011.
(86) Zheng, S.; Javidpour, L.; Sahimi, M.; Shing, K. S.; Nakano, A. SDMD: An Open Source Program for Discontinuous Molecular Dynamics Simulation of Protein Folding and Aggregation. *Comput. Phys. Commun.* **2020**, *247*, 106873.
(87) Zheng, S.; Sajib, M. S. J.; Wei, Y.; Wei, T. Discontinuous Molecular Dynamics Simulations of Biomolecule Interfacial Behavior: Study of Ovispirin-1 Adsorption on a Graphene Surface. *J. Chem. Theory Comput.* **2021**, *17*, 1874−1882.
(88) Ding, F.; Tsao, D.; Nie, H.; Dokholyan, N. V. Ab Initio Folding of Proteins with All-atom Discrete Molecular Dynamics. *Structure* **2008**, *16*, 1010−1018.
(89) Wei, S.; Zou, X.; Tian, J.; Huang, H.; Guo, W.; Chen, Z. Control of Protein Conformation and Orientation on Graphene. *J. Am. Chem. Soc.* **2019**, *141*, 20335−20343.
(90) Xiao, M.; Wei, S.; Chen, J.; Tian, J.; Brooks, C. L., III; Marsh, E. N. G.; Chen, Z. Molecular Mechanisms of Interactions between Monolayered Transition Metal Dichalcogenides and Biological Molecules. *J. Am. Chem. Soc.* **2019**, *141*, 9980−9988.
(91) Wei, S.; Knotts, T. A. A Coarse Grain Model for Protein-Surface Interactions. *J. Chem. Phys.* **2013**, *139*, 095102.
(92) Karanicolas, J.; Brooks, C. L. The Structural Basis for Biphasic Kinetics in the Folding of the WW Domain from a Formin-Binding Protein: Lessons for Protein Design? *Proc. Natl. Acad. Sci. U.S.A.* **2003**, *100*, 3954−3959.
(93) Li, Y.; Wei, S.; Wu, J.; Jasensky, J.; Xi, C.; Li, H.; Xu, Y.; Wang, Q.; Marsh, E. N. G.; Brooks, C. L.; Chen, Z. Effects of Peptide Immobilization Sites on the Structure and Activity of Surface-Tethered Antimicrobial Peptides. *J. Phys. Chem. C* **2015**, *119*, 7146−7155.
(94) Wei, S.; Zou, X.; Cheng, K.; Jasensky, J.; Wang, Q.; Li, Y.; Hussal, C.; Lahann, J.; Brooks, C. L.; Chen, Z. Orientation Determination of a Hybrid Peptide Immobilized on CVD-Based Reactive Polymer Surfaces. *J. Phys. Chem. C* **2016**, *120*, 19078−19086.
(95) Xiao, M.; Wei, S.; Li, Y.; Jasensky, J.; Chen, J.; Brooks, C. L.; Chen, Z. Molecular Interactions between Single Layered MoS_2 and Biological Molecules. *Chem. Sci.* **2018**, *9*, 1769−1773.
(96) Wei, T.; Carignano, M. A.; Szleifer, I. Lysozyme Adsorption on Polyethylene Surfaces: Why Are Long Simulations Needed? *Langmuir* **2011**, *27*, 12074−12081.
(97) Wei, T.; Carignano, M. A.; Szleifer, I. Molecular Dynamics Simulation of Lysozyme Adsorption/Desorption on Hydrophobic Surfaces. *J. Phys. Chem. B* **2012**, *116*, 10189−10194.
(98) Wei, T.; Ma, H.; Nakano, A. Decaheme Cytochrome MtrF Adsorption and Electron Transfer on Gold Surface. *J. Phys. Chem. Lett.* **2016**, *7*, 929−936.
(99) Nakano, C. M.; Ma, H.; Wei, T. Study of Lysozyme Mobility and Binding Free Energy during Adsorption on a Graphene Surface. *Appl. Phys. Lett.* **2015**, *106*, 153701.
(100) Wei, T.; Huang, T.; Qiao, B.; Zhang, M.; Ma, H.; Zhang, L. Structures, Dynamics, and Water Permeation Free Energy across Bilayers of Lipid A and Its Analog Studied with Molecular Dynamics Simulation. *J. Phys. Chem. B* **2014**, *118*, 13202−13209.

https://doi.org/10.1021/acs.jpcb.1c03849
J. Phys. Chem. B 2021, 125, 7706−7716